J Therm Anal Calorim (2016) 125:65–74
DOI 10.1007/s10973-016-5337-6

Physico-chemical characterization of activated carbon–metal oxide photocatalysts by immersion calorimetry in benzene and water

Adrián Barroso-Bogeat[1] · María Alexandre-Franco[1] · Carmen Fernández-González[1] · Vicente Gómez-Serrano[1]

Received: 9 October 2015 / Accepted: 3 February 2016 / Published online: 23 February 2016

Abstract From a commercial activated carbon (AC) and Al^{3+}, Fe^{3+}, Zn^{2+}, $SnCl_2$, TiO_2 and WO_4^{2-} in water, three series of AC–metal (hydr)oxide (MO) samples prepared by wet impregnation in two successive steps of soaking at 80 °C and oven-drying at 120 °C (S1) and subsequent heat treatment at 200 (S2) or 850 °C (S3) were characterized texturally by N_2 adsorption at −196 °C and by immersion calorimetry in benzene and water. The mass changes associated with the preparation of the samples are usually stronger for S1 and S3 than for S2. The incorporation of MO to AC causes a greater decrease in the micropore volume and pore narrowing only for the $SnCl_2$-impregnated sample. The opposite effects on the microporous structure are noted for most S2 and S3, as compared to S1. For AC, $-\Delta_i H(C_6H_6)$ is 114.0 J g^{-1} and $-\Delta_i H(H_2O)$ is 30.5 J g^{-1}. For the AC–MO samples, $-\Delta_i H(C_6H_6)$ and $S_{tot}(C_6H_6)$ are generally lower than for AC and vary by S3 > S2 > S1. However, $-\Delta_i H(H_2O)$, $S_{tot}(H_2O)$ and [O] are usually lower for S3. $S_{tot}(C_6H_6)$ is higher for the samples prepared using the metal ions. The results of immersion calorimetry for AC and AC–MO samples provide one with valuable information concerning the dependence of the hydrophobicity and hydrophilicity of the samples on the method used in their preparation.

Keywords Activated carbon · Metal oxide photocatalysts · Immersion calorimetry · Surface area · Oxygen content

✉ Vicente Gómez-Serrano
vgomez@unex.es

[1] Department of Organic and Inorganic Chemistry, Faculty of Sciences, University of Extremadura, Avda. de Elvas s/n, 06006 Badajoz, Spain

Introduction

Photocatalysis has become an intensively researched field due to practical interest in air and water remediation, self-cleaning surfaces, self-sterilizing surfaces, and hydrogen generation using green energy of sunlight [1]. Semiconductor photocatalysis has been demonstrated to be one of the "green" and effective methods for water and air purification treatments [2]. The photocatalytic process decomposes organic compounds and bacteria into carbon dioxide and water [3]. Many oxide semiconductors show practical performance as photocatalysts in disinfection and detoxification treatments [1]. TiO_2 is by far the most frequently employed photocatalyst owing to the advantages of earth abundance, low toxicity, and thermal and chemical stability [4], besides being cheap, insoluble under most conditions, and photostable [5]. Moreover, TiO_2 in the anatase form is one of the best catalysts for pollutant degradation [6]. Nevertheless, in the mineralization process of organic pollutants such as pentachlorophenol, ZnO also showed high activity, unlike WO_3 and SnO_2 [7]. In photocatalysis reactions, metal oxides such as TiO_2 are generally suspended in the liquid phase or dispersed over high-surface-area materials. The former process is handicapped by filtration of TiO_2 fine particles and effective absorption of ultraviolet–visible radiation. In the latter process, due to their unique pore structure, adsorption capacity, acidity and electronic properties, carbon-based materials of different origins can be used [8]. Among these materials, activated carbon (AC) is the most versatile adsorbent because of its large surface area, polymodal (but essentially microporous) porous structure and variable surface chemical composition [9]. If AC particles are big enough, then filtration is not difficult [10]. For TiO_2 supported on AC, remarkably enhanced decomposition rates of organic compounds were

associated with a high concentration of the organic substrates around the loaded TiO_2 [11].

Semiconductor metal oxides include not only TiO_2 but also Al_2O_3, Fe_2O_3, ZnO, SnO_2 and WO_3. For this broad series of metal oxides supported on AC, the preparation methods and applications were critically reviewed before [12]. More recently, they were used for the removal of mostly synthetic dyes [13–25] and also of other chemical species such as 2,4-dichlorophenoxyacetic acid [26] and Cr(VI) [27]. Previously, using a commercial AC and a wide series of semiconductor metal oxide precursors (i.e. Al^{3+}, Fe^{3+}, Zn^{2+}, $SnCl_2$, TiO_2 and WO_4^{2-}) in water, three series of AC–metal (hydr)oxide (MO) samples were prepared by wet impregnation in two successive soaking and oven-drying steps at low temperatures and by subsequent heat treatment of the resulting samples at higher temperatures. The samples of the three series were characterized in terms of chemical changes and microstructure [28], electrical conductivity [29] and porous texture [30]. The textural study of the samples was undertaken by N_2 adsorption at −196 °C, mercury porosimetry and density measurements.

Although the method of gas physical adsorption at low temperature is the most frequently used in characterization studies of porous solids (i.e. the BET empirical method of calculating specific surface areas is the most popular procedure), such as carbonaceous materials and catalysts, immersion calorimetry in some respects is a complementary one. Immersion calorimetry is a versatile, sensitive and accurate technique which has many advantages [31]. Any change produced not only in surface area and microporosity but also in surface chemistry is amenable to immersion calorimetry. For a given solid/liquid system, the heat of immersion is not only related to the surface area available to the liquid but also to the specific interaction between the solid surface and the immersion liquid [32]. Using non-polar wetting solvents, immersion calorimetry has been used in the characterization of microporous solids [32], such as activated carbons [33, 34] prepared and modified by different methods [35–41]. However, provided that the wetting liquid is an apolar solvent, valuable information concerning the surface functional groups of the carbon and inherently associated properties such as its polar and hydrophilic character can be obtained [42]. On the other hand, the dehydration and dehydroxylation of oxides have also been successfully studied by immersion calorimetry [31]. Metal oxides exhibit specific adsorbent and catalytic activity. They tend to undergo surface hydration and/or hydroxylation as a means of achieving coordinative stabilization. An important consequence of the presence of hydroxyls is that many adsorptive molecules can interact in a specific manner with the surface. In some cases, surface dehydration leads to the exposure of strong cation sites, while other parts of the surface may become reactive. The possible types of specific interactions include hydrogen bonding and Lewis electron acceptor–donor exchange [31].

For use in the characterization of metal oxide photocatalysts supported on AC intended for water purification, immersion calorimetry is clearly advantageous as compared to gas adsorption. Immersion calorimetry spans more respects of the composite catalyst that are particularly relevant to the adsorption of solutes from water. Furthermore, because of capillarity phenomena in pores of the carbon support, the use of liquids as the solvent both in the characterization of the catalyst and in the adsorption of organic pollutants for their degradation and removal renders immersion calorimetry a more reliable analysis tool. This also holds for the size of adsorptives, regarding its influence on accessible porosity and adsorbability. Molecular sieve effects, which may be enhanced by the presence of a metal catalyst in pores of the carbon support, may be more amenable to the analysis by immersion calorimetry.

Immersion calorimetry has been widely used in textural and surface studies of AC [32, 43–46]. For AC–metal oxides, however, it has been done only rarely [47]. Hence, using such an analysis tool, the present study was primarily focused on the analysis of the three series of prepared AC–MO catalysts by immersion calorimetry. Since these heterogeneous catalysts, which are made up of AC and unevenly surface dispersed MO, were prepared from various MO precursors by heating under different conditions, it was expected that they greatly differ from their chemical composition and thereby calorimetric behaviour. Benzene and water were chosen as immersion liquids in order to measure immersion enthalpies by discriminating between heat effects due to hydrophobic and hydrophilic interactions.

Experimental

Materials and reagents

A granular AC from Merck® (Darmstadt, Germany), 1.5-mm average particle size (Cod. 1.02514.1000), as received, was used as support for Al_2O_3, Fe_2O_3, ZnO, SnO_2, TiO_2 and WO_3 . The selected precursors of these catalysts were $Al(NO_3)_3{\cdot}9H_2O$, $Fe(NO_3)_3{\cdot}9H_2O$, $Zn(NO_3)_2{\cdot}6H_2O$, $SnCl_2{\cdot}2H_2O$ and $Na_2WO_4{\cdot}2H_2O$, all of them purchased from Panreac® (Barcelona, Spain) and being of reagent grade. As an exception to the rule, anatase powder (Aldrich®; Steinheim, Germany), particle size lower than 44 μm, was used for TiO_2.

Sample preparation

The preparation of the AC–MO samples was performed as described in detail elsewhere [28–30] and briefly summarized in Table 1, which also lists the sample codes. As a whole, three series of samples were prepared (i.e. three samples for each metal oxide precursor): S1, soaking at 80 °C for 5 h and oven-drying at 120 °C for 24 h; S2, S3, subsequent heating of S1 at 200 °C or 850 °C for 2 h, respectively. The yield of the preparation process of the AC–MO samples was estimated by the following expression:

$$\text{Yield(mass\%)} = \frac{M_f}{M_i} \times 100 \quad (1)$$

where M_i stands for the mass either of AC (i.e. 25 g) or of samples S1, whereas M_f denotes the mass of final product after oven-drying at 120 °C or heat-treating at 200 or 850 °C. The yield values are given in Table 2.

Sample characterization

By N_2 adsorption at −196 °C

The textural characterization of the samples was undertaken by N_2 adsorption at −196 °C, mercury porosimetry and helium and mercury density measurements [30]. From the experimental N_2 adsorption isotherms, the apparent surface area (S_{BET}) was calculated by applying the Brunauer, Emmet and Teller equation (BET) [48]. Furthermore, by using the Dubinin–Radushkevich (D–R) equation [49], the micropore volume (W_0), characteristic energy (E_0), average pore width (L_0) of ideally slit-shaped micropores, and surface area of their walls (S_{mi}) were calculated. On the other hand, the comparison plot developed by Setoyama et al. [50, 51] allows one to calculate both the total surface area (S_{comp}) and the external (non-microporous) surface area (S_{ext}) of the carbon sample by comparing its N_2 adsorption isotherm with the data for a non-porous carbon reference (typically a carbon black such as Vulcan 3G, 80 $m^2\ g^{-1}$ [52, 53]). Then, the total surface area (S_{tot}) of the solid was estimated from:

$$S_{tot} = S_{mi} + S_{ext} \quad (2)$$

The calculated values of S_{BET}, W_0 and L_0 were reported before [30], and those of S_{mi}, S_{ext} and S_{tot} are collected in Table 2.

By immersion calorimetry

Immersion calorimetry experiments were carried out in two identical calorimeters of the Tian–Calvet type, specifically designed for working with carbon materials and measuring absolute energies in the range from 2 to 20 J [54, 55]. In a typical experiment, 0.025–0.080 g of sample was weighed in a glass bulb with a tiny brittle end and it was out-gassed under a pressure of 133.3×10^{-5} Pa for 6–10 h at 110 °C. Afterwards, the bulb was sealed and attached to a stainless steel rod through a close fitting of the same material. This assembly was introduced into the calorimetric cell containing 5 mL of the wetting liquid (i.e. benzene or water) and carefully closed by means of an O-ring seal. Then, the system was placed inside the calorimeter block and enough time was left for temperature equilibration between the sample set-up and the calorimeter. Once the thermal equilibrium was reached, the rod was gently depressed to break the brittle end of the bulb with the bottom of the calorimetric cell, thus allowing the liquid to enter the bulb and wet the carbon sample. As a result of the wetting process, a given amount of heat was released and its evolution was monitored as a function of time over 30–45 min. Integration of the resulting curve provided the experimental immersion enthalpy into the liquid. Reproducibility of results was provided by a periodic check of the calibration of the calorimeter carried out by means of the immersion of activated carbon U-03 in benzene; its value of the immersion enthalpy (i.e. -128.8 ± 15 J g^{-1}) is considered as standard. Deviations of the order of 10 % or less with respect to the reference value were obtained experimentally.

From the measured enthalpies of immersion into benzene and water, $\Delta_i H(C_6H_6)$ and $\Delta_i H(H_2O)$, the total surface area of the samples accessible to both wetting liquids was calculated by the expressions (3) and (4):

$$S_{tot}(C_6H_6) = \frac{-\Delta_i H(C_6H_6)}{0.114} \quad (3)$$

$$S_{tot}(H_2O) = \frac{-\Delta_i H(H_2O)}{0.045} \quad (4)$$

The constant 0.114 stands for the average specific enthalpy of immersion for graphitized carbon blacks in benzene [33], while the 0.045 is the average specific enthalpy of immersion obtained for six activated carbons

Table 1 Preparation of the AC–MO catalysts: codes

Precursor	pH	Heat treatment temperature		
		120 °C	200 °C	850 °C
$Al(NO_3)_3{\cdot}9H_2O$	2.91	A120	A200	A850
$Fe(NO_3)_3{\cdot}9H_2O$	1.54	F120	F200	F850
$Zn(NO_3)_2{\cdot}6H_2O$	5.16	Z120	Z200	Z850
$SnCl_2{\cdot}2H_2O$	1.37	S120	S200	S850
TiO_2 anatase	5.84	T120	T200	T850
$Na_2WO_4{\cdot}2H_2O$	9.54	W120	W200	W850

Table 2 Preparation and characterization of the samples: yield, textural and immersion calorimetry data

Series	Sample	Yield/%	L_0/nm	S_{mi}/m^2 g^{-1}	S_{ext}/m^2 g^{-1}	S_{tot}/m^2 g^{-1}	$-\Delta_i H(C_6H_6)$/J g^{-1}	$S_{tot}(C_6H_6)$/m^2 g^{-1}	$-\Delta_i H(H_2O)$/J g^{-1}	$S_{tot}(H_2O)$/m^2 g^{-1}	[O]/mmol g^{-1}
	AC		1.00	720	55	775	114.0	1000	30.5	677	0.65
Series 1	A120	102	1.05	590	52	642	69.3	608	47.6	1057	3.30
	F120	114	0.99	586	42	628	83.3	731	70.1	1557	5.26
	Z120	103	1.02	588	49	637	114.3	1003	56.1	1247	3.21
	S120	149	0.92	304	23	327	30.4	267	33.4	742	2.70
	T120	103	1.00	700	59	759	111.1	974	31.5	701	0.82
	W120	106	0.99	646	52	698	104.7	919	26.0	577	0.40
Series 2	A200	93	1.06	509	39	548	103.3	906	66.6	1479	4.49
	F200	94	1.02	569	35	604	99.9	876	65.4	1453	4.45
	Z200	91	0.97	639	51	690	83.0	728	49.1	1091	3.17
	S200	96	1.11	270	22	292	37.6	330	50.6	1124	4.27
	T200	96	1.12	625	51	676	96.3	844	34.6	768	1.43
	W200	96	1.04	615	46	661	126.5	1109	25.0	555	–
Series 3	A850	90	1.32	515	57	572	110.9	973	30.6	680	0.73
	F850	81	1.11	559	37	596	106.2	931	23.0	511	0.07
	Z850	84	1.08	593	62	655	75.2	659	29.7	660	1.39
	S850	68	1.13	584	41	625	63.1	554	31.0	690	1.10
	T850	98	1.35	548	58	606	66.9	586	21.4	475	0.62
	W850	95	1.14	614	50	664	114.5	1004	32.1	713	0.72

prepared under similar conditions from bituminous coal and anthracite [33].

As reported elsewhere [56, 57], immersion calorimetry into benzene and water also allows us to estimate the total content of surface oxygen for the samples ([O]) by the following expression:

$$[\mathrm{O}]\left(\mathrm{mmol\,g^{-1}}\right) = \frac{0.21 \cdot \Delta_i H(\mathrm{C_6H_6}) - \Delta_i H(\mathrm{H_2O})}{10} \qquad (5)$$

The values of $-\Delta_i H(C_6H_6)$, $-\Delta_i H(H_2O)$, $S_{tot}(C_6H_6)$, $S_{tot}(H_2O)$ and [O] obtained for AC and the three series of AC–MO samples are listed in Table 2. These values are always given by an average of the results of three measurements under identical conditions.

Results and discussion

Preparation of the samples: process yield

From the yield values in Table 2, it follows that the mass change produced as a result of the process of preparation of the samples is strongly dependent on the MO precursor and heating conditions. As regards samples S1, the mass gain is greater by the order S120 > F120 > W120 > Z120 ≈ T120 > A120. Probably, a major factor with influence on the mass of sample was the size of the MO precursor in the impregnation solution, because of the control of diffusion in AC pores. Such a size will be smaller by hydroxo-complexes < aquo-complexes < polymeric species < colloidal particles. In accordance with the process yields, diffusion was more favourable for $SnCl_2$, Fe^{3+} and WO_4^{2-}. However, the opposite applies to Al^{3+}, Zn^{2+} and TiO_2. For samples S2 and S3, yield ranges between 91 and 96 mass% and between 68 and 98 mass%, respectively. Since these series of samples were prepared by heating samples S1 at 200 or 850 °C, the mass decrease should be mainly due to dehydration for samples S2 and to dehydroxylation, carbothermal reduction and other thermal processes for samples S3. Overall, except for S850, these processes occurred to a larger extent when the metal ions (Al^{3+}, Fe^{3+} and Zn^{2+}) were used in the preparation of samples S1. The reduction of a metal oxide (M_nO_m) by carbon at high temperature (i.e. the so-called carbothermal reduction) may be written as:

$$M_nO_m + mC \rightarrow nM + mCO \qquad (6)$$

$$2CO \rightarrow C + CO_2 \qquad (7)$$

and forms elemental metal and carbon monoxide, which was released with an enhanced mass loss and lower yield. At high heat temperature, CO may disproportionate into C and CO_2 by the reaction (7). The lower yields for F850 and S850 are in line with the greater presence of MO in F120 and S120 than for the rest of the samples. In connection with the mass loss produced for samples S3, it should be also taken into account the lower melting point of 231.93 °C for Sn, 419.53 °C for Zn and 660.32 °C for Al [58] than 850 °C (i.e. maximum heat treatment temperature in the preparation of these samples) since consequently these metals, after formation by the reaction (6), should melt and vaporize. By contrast, Fe and W that melt at 1538 and 3414 °C, respectively, should remain physically unaltered in the samples. Likewise, the high yield obtained for T850 is consistent with the high thermal and chemical stability of this substance [59].

Microporosity and surface area

As compared to AC (L_0, 1.00 nm; W_0, 0.36 $cm^3\ g^{-1}$ [30]), for a number of samples S1, L_0 and W_0 are only slightly different, and therefore it may be stated that impregnation as a rule hardly affected the microporous structure of AC. This was so in particular for T120 (W_0, 0.35 $cm^3\ g^{-1}$) [30], which may be connected with the large size of anatase colloidal particles and consequent accessibility of the microporous structure of this sample to N_2 at −196 °C. The exceptions to the rule arise from A120, F120 and S120. In the case of A120, the noticeable L_0 increase and W_0 (0.31 $cm^3\ g^{-1}$) [30] decrease suggest that the catalyst precursor cumulated in the entrances of small micropores of the carbon, a fraction of its porosity becoming then inaccessible even to a small molecule as N_2. For F120 (W_0, 0.29 $cm^3\ g^{-1}$) and S120 (W_0, 0.14 $cm^3\ g^{-1}$) [30], the L_0 and W_0 decreases are in line with the loading of a larger amount of MO precursor during their preparation, as shown by high yields obtained for these samples. Notice that it is accompanied with a more marked pore narrowing only for S120. On the other hand, the values of L_0 for samples S2 and S3 indicate that the heat treatment of samples S1 at 200 or 850 °C originated microporosity widening, the effect being stronger for samples S3 than for samples S2.

The BET surface area (S_{BET}) is 711 $m^2\ g^{-1}$ for AC [30]. For the AC–MO samples, in general, S_{BET} is larger for samples S3 than for samples S1. Thus, S_{BET} is 278 $m^2\ g^{-1}$ for S120 and 680 $m^2\ g^{-1}$ for S850 [30]. For the samples prepared with TiO_2, S_{BET} is higher than for AC and varies by T850 (847 $m^2\ g^{-1}$) > T200 (776 $m^2\ g^{-1}$) ≈ T120 (780 $m^2\ g^{-1}$) [30]. The S_{BET} increase for T850 may be surprising as a strong effect of total porosity reduction was previously reported by Blanco et al. [60] when TiO_2 was heat-treated at 800 and 1000 °C. Therefore, the development of surface area for T850 is attributable to physical or chemical changes suffered by T120 as a result of the preparation of T850. Thus, processes such as disruption of hydrogen bonding between surface –OH groups and

dehydroxylation likely occurred, increasing the porosity accessible to the N_2 molecule in the sample. It should be noted that there was also an accused porosity widening as L_0 is 1.0 nm for T120, 1.12 nm for T200 and 1.35 nm for T850. The deviation of S_{tot} from S_{BET} is commonly small, which agrees with the L_0 values of around 1.00 nm obtained for most samples as it was previously reported that S_{BET} and the real surface area $S_{mi} + S_{ext}$ are in agreement only for carbons with average pore widths L_0 around 0.8–1.1 nm [34]. The percentage of relative variation for S_{BET} and S_{tot}, as referred to S_{BET}, is usually lower than 10 %. Two exceptions to the rule are A850 and T850 for which L_0 is 1.32 and 1.35 nm and such a percentage is as high as 24.6 and 28.5, respectively. As a rule, S_{BET} is lower and higher than S_{tot} for samples S1 and samples S3, respectively.

Results of immersion calorimetry

Enthalpies in benzene: surface areas

After contact between the solid and liquid phases was established in an immersion calorimetry measurement, because of its apolar character, the benzene molecule should prefer to take part in hydrophobic interactions with graphene layers rather than with surface functional groups of AC and AC-supported MO, as MO is hydrophilic in character. The immersion enthalpy of the samples in benzene, $-\Delta_i H(C_6H_6)$, should be therefore higher for samples containing lower contents of oxygen surface groups and MO. Furthermore, it should be taken into account that the hydrophilic character of AC-supported MO will depend on whether it was found as an aquo- or hydroxo-complex or as a metal oxide. In the latter case, hydrophilicity is customarily associated with the metal–oxygen bond ionicity. Of course, as heat treatment temperature increased in the preparation of the samples, an irreversible removal of oxygen surface groups from AC and of water, hydroxyl groups and oxygen from MO should tend to increase the hydrophobic character in the resulting product. This statement also holds for the thermal degradation of oxygen surface groups of AC, both indigenous and artificially formed because of its interaction with the MO loaded on its surface. Therefore, as a rough approximation, one may look on the relative mass of the effects associated with AC and MO on hydrophobicity as a function of the amount of MO loaded on AC, which is given by the process yield. In brief, because of its relationship with the hydrophobicity, the measured $-\Delta_i H(C_6H_6)$ provides one with valuable information concerning the ability of a given sample to adsorb photosensitive organic molecules of environmental interest.

As shown by data in Table 2, $-\Delta_i H(C_6H_6)$ as a rule is lower for samples S1 than for AC (i.e. between 30.4 and 114.3 and 114.0 J g^{-1}, respectively), as expected because

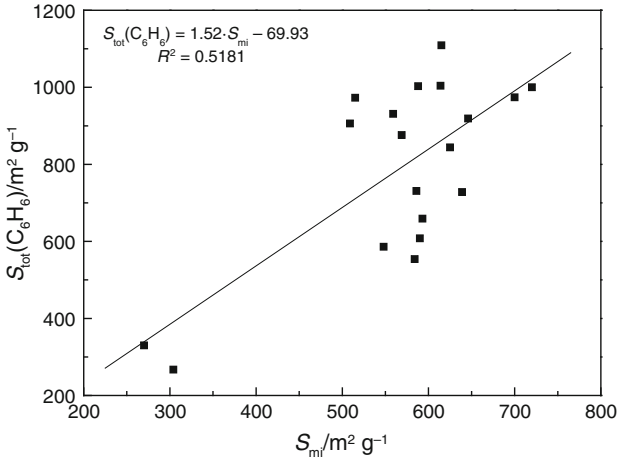

Fig. 1 Immersion enthalpies in benzene. Plot of $S_{tot}(C_6H_6)$ against S_{mi}

of the incorporation of hydrophylic oxygen-containing metal species to AC. It is so in particular when $SnCl_2$ was used in the preparation of S120. In connection with the lower $-\Delta_i H(C_6H_6)$ for F120 and A120 than for Z120, it is relevant to point out that the tendency to hydrolysis shown by the metal ions is much higher for the Fe^{3+} and Al^{3+} ions than for the Zn^{2+} ion [61], as proved by the pH of the impregnation solutions (see data in Table 1). However, it should be also noted that hydrolysis is a more favourable process for the Fe^{3+} ion than for the Al^{3+} ion and that $-\Delta_i H(C_6H_6)$ is markedly higher for F120 than for A120. Furthermore, the greater presence of MO precursor in F120 than in A120 should also give rise to a higher $-\Delta_i H(C_6H_6)$ for A120. Accordingly, the noticeably lower $-\Delta_i H(C_6H_6)$ for A120 is compatible with a more restricted access of A120 microporosity to the C_6H_6 molecule because of the cumulation of Al^{3+} chemical species in micropore

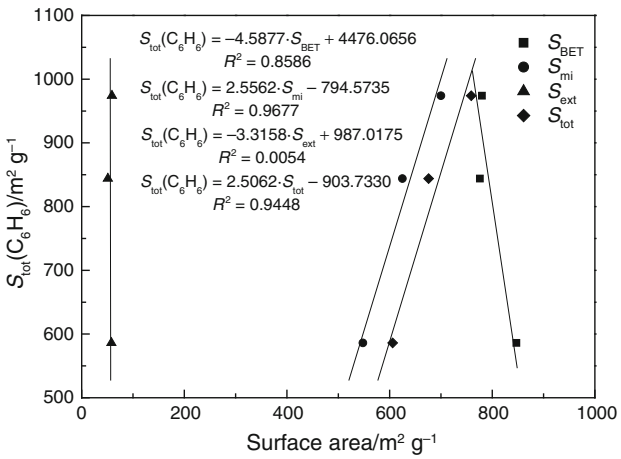

Fig. 2 Immersion enthalpies in benzene. Plot of $S_{tot}(C_6H_6)$ against various textural parameters for the AC–TiO_2 samples

entrances of AC, as described above. With the temperature rise in the preparation of the samples (i.e. from 120 to 200 or 850 °C), $-\Delta_i H(C_6H_6)$ increased for Al^{3+}, Fe^{3+} and $SnCl_2$, decreased for Zn^{2+} and TiO_2, and first increased and then decreased for WO_4^{2-}. The $-\Delta_i H(C_6H_6)$ decrease may be associated with thermal desorption processes involving less hydrophilic atomic groupings, leading to concentration of more hydrophilic groups in the resulting product (e.g. removal of water molecules to the benefit of hydroxyl groups). In fact, the greater $-\Delta_i H(C_6H_6)$ decrease for T850 than for T200 is compatible with a progressive increase in the content of TiO_2 in the sample as temperature increased in its preparation. Conversely, the $-\Delta_i H(C_6H_6)$ increase for W850 as compared to W120 can be accounted for by a decreased presence of WO_3 in the sample after heat treatment at high temperature. In brief, from the results of immersion calorimetry into benzene it becomes apparent that by impregnating AC with Al^{3+}, Fe^{3+}, Zn^{2+}, $SnCl_2$, TiO_2 and WO_4^{2-} in water and subsequent heating at higher temperatures a large number of samples of broadly varying hydrophobicity, which is usually lower than for AC, can be prepared.

As calculated by the expression (3), $S_{tot}(C_6H_6)$ is proportional to $-\Delta_i H(C_6H_6)$ and therefore the variation tendencies of both quantities are the same for the various series of samples. The plots of $S_{tot}(C_6H_6)$ against W_0, S_{BET}, S_{mi}, S_{ext} and S_{tot} show a positive correlation, which is consistent with an increase in the available hydrophobic surface of AC in the AC–MO samples as these textural parameters increase. Data fit better to a straight line with R^2 somewhat higher than 0.50 for S_{tot} and S_{mi}, as depicted in Fig. 1. However, the opposite applies when $S_{tot}(C_6H_6)$ is plotted *versus* W_0, S_{ext} or S_{BET}, with R^2 being then in turn approximately 0.44, 0.26 and 0.31. Of course, for samples prepared from an individual MO precursor, fittings with R^2 values closer to unity are usually obtained. As a guide, it is shown in Fig. 2 for the three TiO_2-containing samples.

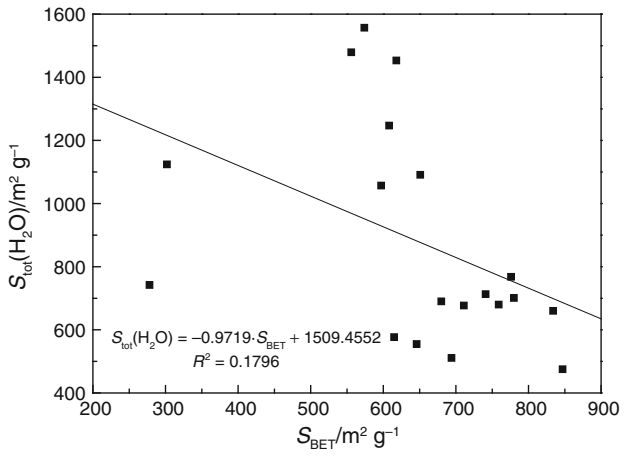

Fig. 3 Immersion enthalpies in water. Plot of $S_{tot}(H_2O)$ against S_{BET}

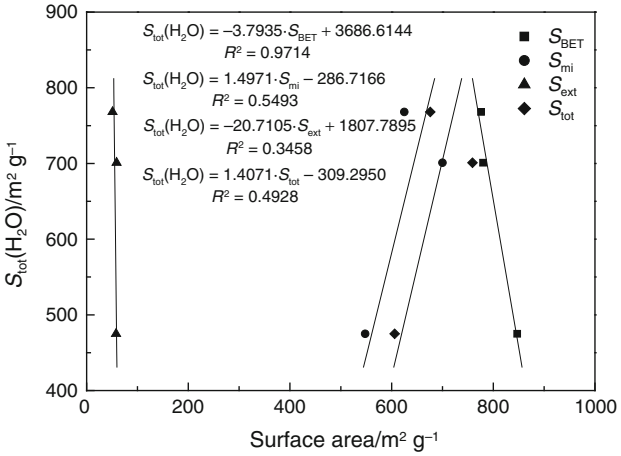

Fig. 4 Immersion enthalpies in water. Plot of $S_{tot}(H_2O)$ against various textural parameters for the AC–TiO_2 samples

Enthalpies in water: surface areas

In the case of water, which is a polar molecule unlike benzene, the incorporation of hydrophilic groups (i.e. oxygen surface groups of AC and coordination groups and polarized bonds present in MO) to AC in the preparation of samples S1 and their subsequent removal from samples S1 in the preparation of samples S2 and S3 should result in an $-\Delta_i H(H_2O)$ increase and decrease, respectively. The values of $-\Delta_i H(H_2O)$ in Table 2 show that $-\Delta_i H(H_2O)$ is 30.5 J g^{-1} for AC and between 21.4 J g^{-1} for T850 and 70.1 J g^{-1} for F120. As expected, $-\Delta_i H(H_2O)$ is usually higher for the AC–MO samples than for AC. Also, it is higher for samples S1 and S2 prepared using metal ions as MO precursors. Thus, $-\Delta_i H(H_2O)$ varies by F120 > A200 > F200 > Z120, and so on. For the various series of samples, the maximum $-\Delta_i H(H_2O)$ and thereby hydrophilicity follow the sequence F120 > A200 ≫ W850. Therefore, from F120 to W850 in this series of samples either the number or strength of the hydrophilic groups should decrease. Notice that $-\Delta_i H(H_2O)$ is higher for the samples prepared using the metal ions. For these samples, it is also noted a more marked influence of heat treatment temperature on $-\Delta_i H(H_2O)$ than for the samples prepared with TiO_2 and WO_4^{2-}. In short, AC–MO samples that are more hydrophilic in character can be prepared using metal ions and operating at low temperatures.

The $S_{tot}(H_2O)$ values, as calculated by the expression (4), are compiled in Table 2. The plots of $S_{tot}(H_2O)$ against the textural parameters derived from the N_2 adsorption isotherms (as an illustrative example, see Fig. 3) show negative correlations. It may be accounted for by an increased hydrophilicity and simultaneous detrimental effects on

porosity and surface area with the increase in the MO content of the samples. Contrary to $S_{tot}(C_6H_6)$, in the case of $S_{tot}(H_2O)$ correlations are worse when S_{mi} and S_{tot} are used on the X-axis. Figure 4 shows the plots obtained for the samples prepared using TiO_2.

Comparison of immersion enthalpies: oxygen content

For ACs prepared from lignocellulosic materials by physical and chemical activations, the reported values of $-\Delta_i H(C_6H_6)$ are 109.7 J g^{-1} (i.e. for the carbon H25) [40, 62] and between 4.0 and 181.1 J g^{-1} [44–46] and of $-\Delta_i H(H_2O)$ are 29.7 J g^{-1} [40, 62] and between 7.4 and 67.01 J g^{-1} [44, 46] which, as compared to the respective values of 114.0 and 30.5 J g^{-1} obtained for AC (data in Table 2), show that they are very similar or different depending on the carbon. From the $-\Delta_i H(C_6H_6)$ values, it follows that the degree of development of surface area is a decisive factor in relation to the amount of evolved heat after the immersion of the carbon in C_6H_6. As far as $-\Delta_i H(H_2O)$ is concerned, its magnitude seems to be mainly dependent on the surface functional groups as $-\Delta_i H(H_2O)$ is similar for carbonaceous products with very different surface developments. On the other hand, it was found that for activated carbon modified with CuO $-\Delta_i H(H_2O)$ is markedly influenced by the concentration of the Cu^{2+} solution used in the impregnation of the carbon [47].

Comparison of $-\Delta_i H(C_6H_6)$ and $-\Delta_i H(H_2O)$ gives some insight into the relative changes produced in the hydrophobic and hydrophilic characters of AC because of the loading of metal (hydr)oxide photocatalysts. In principle, as stated above, it was expected that as the content of MO loaded on AC increased, $-\Delta_i H(C_6H_6)$ decreased and $-\Delta_i H(H_2O)$ increased. However, it should be taken into account that the enthalpic effects associated with the immersion process are also a function of the composition changes originated during the preparation of the samples, because of the influence of specific interactions with the immersion liquid on heat release. As compared to AC (see $-\Delta_i H$ data in Table 2), $-\Delta_i H(C_6H_6)$ is lower and $-\Delta_i H(H_2O)$ is higher for most AC–MO samples. However, a greater $-\Delta_i H(C_6H_6)$ decrease is not accompanied with a greater $-\Delta_i H(H_2O)$ increase, and vice versa. As a guide, it can be noted that both $-\Delta_i H(C_6H_6)$ and $-\Delta_i H(H_2O)$ are higher for F120 than for A120, whereas they are lower for S120 than for A120. Therefore, it seems that the strength of the specific interactions of the samples with the wetting liquid rather than the number of interactions was the dominant factor in controlling the amount of heat release as a result of the immersion process in the calorimetry run. For samples S2 and S3, the expected $-\Delta_i H(C_6H_6)$ increase and $-\Delta_i H(H_2O)$ decrease with increasing heat treatment temperature only appear for the samples prepared with Al^{3+}, Fe^{3+} and $SnCl_2$. However, the opposite variation of $-\Delta_i H(C_6H_6)$ is observed for the samples prepared with TiO_2 and Zn^{2+}, although $-\Delta_i H(H_2O)$ follows the sequences T120 < T200 > T850 and Z120 > Z200 > Z850.

According to the expression (5), the calculated oxygen content for the samples is mainly a function of $-\Delta_i H(H_2O)$ instead of $-\Delta_i H(C_6H_6)$. Therefore, the obtained [O] gives one a rough idea of the oxygen accessible to water that is further hydrophilic in character. In all likelihood, the calculated [O] by the expression (5) is different from the total amount of oxygen present in the samples. In fact, in this connection it should be recalled here that the samples were out-gassed under prefixed vacuum and heating conditions and that thereby hydration water was surely removed from the samples, prior to effecting enthalpy measurements. Data in Table 2 show that [O] as a rule is much higher for samples S1 than for AC, which is consistent with the incorporation of coordinatively bound oxygen for the metal ions and of structural oxygen for the metal oxides to AC during the preparation of the samples. For couples of homologous samples, [O] is usually quite similar for samples S1 and S2 and much lower for samples S3. For the various series of samples, the highest [O] appears for F120 (5.26 mmol g^{-1}), A200 (4.49 mmol g^{-1}) and Z850 (1.39 mmol g^{-1}). Then, the results obtained for samples S1 and S2 argue for a rather uniform chemical surface as far as the chemical nature and content of hydrophilic groups are concerned. Perhaps, the effects on the chemical composition of samples S1 due to heat treatment at 200 °C in the preparation of samples S2 and to outgassing at 110 °C in the calorimetry tests were similar. On the contrary, the heat treatment of samples S1 at 850 °C in the preparation of samples S3 produced a strong decrease in the content of the hydrophilic groups because of occurrence of irreversible processes such as dehydroxylation and carbothermal reduction. The very low [O] in particular for F850 is worth mentioning as it may be associated with the presence of elemental Fe instead of an iron oxide in the sample. For T850, W850 and A850, the [O] is similar to that for AC. Therefore, from these results it becomes evident that by heat treatment of samples S1 at 850 °C samples with a re-established hydrophobic character as compared to AC are obtained.

Conclusions

From the above results obtained first in the preparation of three series of AC–MO samples by the wet impregnation method in two soaking and oven-drying steps and subsequent heat treatment and then in the characterization of the resulting samples by immersion calorimetry in benzene and water, the following conclusions may be drawn.

The yield of the process of preparation of the AC–MO samples is strongly dependent on the impregnation agent and heat treatment temperature. For samples S1, it is higher in particular for F120 and especially for S120, contrarily to A120, Z120 and T120. As compared to samples S1, the yield variation is greater for samples S3 than for samples S2. For samples S3, it is lower by S850 < F850 < Z850 < A850 < W850 < T850 and varies in the range 68 mass% for S850 and 98 mass% for T850. The incorporation of the metal (hydr)oxides to AC results in W_0 decrease. The effect is stronger and is accompanied with a greater pore narrowing only for S120. However, the opposite effects on the microporous structure are observed for most samples S2 and S3 with respect to samples S1. For AC, $-\Delta_i H(C_6H_6)$ is 114.0 J g^{-1} and $-\Delta_i H(H_2O)$ is 30.5 J g^{-1}. For the AC–MO samples, $-\Delta_i H(C_6H_6)$ and $S_{tot}(C_6H_6)$ are usually lower than for AC; $-\Delta_i H(C_6H_6)$ being 30.4 J g^{-1} for S120. For samples S3, as compared to samples S1, the general tendency of $-\Delta_i H(C_6H_6)$ is to increase. $-\Delta_i H(H_2O)$ and $S_{tot}(H_2O)$ as a rule are higher for samples S1 and S2 than for AC, $-\Delta_i H(H_2O)$ being 70.1 J g^{-1} for F120. For samples S3, they are similar or lower than for AC. The [O] is usually higher for the AC–MO samples than for AC, especially for samples S1 and S2, whereas for samples S3 it becomes closer to that for AC. By the simple method of wet impregnation and heat treatment, a variety of samples with a wide range of surface properties concerning their hydrophobic and hydrophilic characters are prepared. Therefore, valuable information in relation to the use of the samples as adsorbents and catalysts in photocatalytic processes is obtained.

Acknowledgements Financial support by Gobierno de Extremadura and European FEDER Funds is gratefully acknowledged. A. Barroso-Bogeat thanks Spanish Ministerio de Educación, Cultura y Deporte for the concession of a FPU Grant (AP2010-2574). Authors are deeply grateful to T.A. Centeno and B. Lobato-Ortega (INCAR-CSIC, Oviedo) for their kind assistance throughout the calorimetry experiments.

References

1. Li WX. Photocatalysis of oxide semiconductors. J Aust Ceram Soc. 2013;49:4–6.
2. Yu J, Trapalis C, Zhang P, Li G, Yu H. Environmental photocatalysis 2013. Int J Photoenergy. 2013;. doi:10.1155/2013/786806.
3. Fujishima A, Zhang X, Tryk DA. TiO_2 photocatalysis and related surface phenomena. Surf Sci Rep. 2008;63:515–82.
4. Zhang M, Wu J, Lu DD, Yang J. Enhanced visible light photocatalytic activity for TiO_2 nanotube array films by co-doping with tungsten and nitrogen. Int J Photoenergy. 2013;. doi:10.1155/2013/471674.
5. Mills A, Davies RH, Worsley D. Water purification by semiconductor photocatalysis. Chem Soc Rev. 1993;22:417–25.
6. Bickley RI, Gonzalez-Carreno T, Lees JS, Palmisano L, Tilley RJD. A structural investigation of titanium dioxide photocatalysts. J Solid State Chem. 1991;92:178–90.
7. Barbeni M, Pramauro E, Pelizzetti E. Photodegradation of pentachlorophenol catalyzed by semiconductor particles. Chemosphere. 1985;14:195–208.
8. Faria JL, Wang W. Carbon materials in photocatalysis. In: Serp P, Figueiredo JL, editors. Carbon materials for catalysis. Hoboken: Wiley; 2009. p. 481–506.
9. Rodríguez-Reinoso F. Activated carbon: structure, characterization, preparation and applications. In: Marsh H, Heintz EA, Rodríguez-Reinoso F, editors. Introduction to carbon technologies. Alicante: Universidad de Alicante; 1997. p. 35–101.
10. El-Sheikh AH, Newman AP, Al-Daffaee H, Phull S, Cresswell N, York S. Deposition of anatase on the surface of activated carbon. Surf Coat Technol. 2004;187:284–92.
11. Takeda N, Torimoto T, Sampath S, Kuwabata S, Yoneyama H. Effect of inert supports for titanium dioxide loading on enhancement of photodecomposition rate of gaseous propionaldehyde. J Phys Chem. 1995;99:9986–91.
12. Barroso-Bogeat A, Fernández-González C, Alexandre-Franco M, Gómez-Serrano V. Activated carbon as a metal oxide support: a review. In: Kwiatkowski JF, editor. Activated carbon: classifications, properties and applications. New York: Nova Science; 2011. p. 297–318.
13. García JC, Castellanos MP, Uscátegui A, Fernández J, Pedroza AM, Daza CE. Remoción de colorantes sintéticos mediante el proceso Fenton heterogéneo usando Fe_2O_3 soportado en carbón activado obtenido a partir de residuos de rosas. Universitas Scientiarum. 2012;17:303–14.
14. Kadirova ZC, Katsumata K, Isobe T, Matsushita N, Nakajima A, Okada K. Adsorption and photodegradation of methylene blue with Fe_2O_3-activated carbons under UV illumination in oxalate solution. J Environ Chem Eng. 2014;2:2026–36.
15. Changsuphan A, Wahab MIBA, Oanh NTK. Removal of benzene by ZnO nanoparticles coated on porous adsorbents in presence of ozone and UV. Chem Eng J. 2012;181–182:215–21.
16. Chen J, Wen X, Shi X, Pan R. Synthesis of zinc oxide/activated carbon nano-composites and photodegradation of rhodamine B. Environ Eng Sci. 2012;29:392–8.
17. Muthirulan P, Meenakshisundararam M, Kannan N. Beneficial role of ZnO photocatalyst supported with porous activated carbon for the mineralization of alizarin cyanin green dye in aqueous solution. J Adv Res. 2013;4:479–84.
18. Gao B, Yap PS, Lim TM, Lim TT. Adsorption-photocatalytic degradation of acid red 88 by supported TiO_2: effect of activated carbon support and aqueous anions. Chem Eng J. 2011;171:1098–107.
19. Slimen H, Houas A, Nogier JP. Elaboration of stable anatase TiO_2 through activated carbon addition with high photocatalytic activity under visible light. J Photochem Photobiol A. 2011;221:13–21.
20. Huang D, Miyamoto Y, Matsumoto T, Tojo T, Fan T, Ding J, Guo Q, Zhang D. Preparation and characterization of high-surface-area TiO_2/activated carbon by low-temperature impregnation. Sep Purif Technol. 2011;78:9–15.
21. Jamil TS, Ghaly MY, Fathy NA, Ab del-halim TA, Österlund L. Enhancement of TiO_2 behavior on photocatalytic oxidation of MO dye using TiO_2/AC under visible irradiation and sunlight radiation. Sep Purif Technol. 2012;98:270–9.
22. Asiltürk M, Sener S. TiO_2-activated carbon photocatalysts: preparation, characterization and photocatalytic activities. Chem Eng J. 2012;180:354–63.
23. Mahadwad OK, Parikh PA, Jasra RV, Patil C. Photocatalytic degradation of reactive black-5 dye using TiO_2-impregnated active carbon. Environ Technol. 2012;33:307–12.

24. Mahlambi MM, Mishra AK, Mishra SB, Krause RW, Mamba BB, Raichur AM. Effect of metal ions (Ag Co, Ni, and Pd) on the visible light degradation of rhodamine B by carbon-covered alumina-supported TiO2 in aqueous solutions. Ind Eng Chem Res. 2013;52:1783–94.
25. Ouzzine M, Romero-Anaya AJ, Lillo-Ródenas MA, Linares-Solano A. Spherical activated carbon as an enhanced support for TiO_2/AC photocatalysts. Carbon. 2014;67:104–18.
26. Rivera-Utrilla J, Sánchez-Polo M, Abdel Daiem MM, Ocampo-Pérez R. Role of activated carbon in the photocatalytic degradation of 2,4-dichlorophenoxyacetic acid by the UV/TiO_2/activated carbon system. Appl Catal B. 2012;126:100–7.
27. Shaban YA. Effective photocatalytic reduction of Cr(VI) by carbon modified (CM)-n-TiO_2 nanoparticles under solar irradiation. World J Nano Sci Eng. 2013;3:154–60.
28. Barroso-Bogeat A, Alexandre-Franco M, Fernández-González C, Gómez-Serrano V. Preparation and microstructural characterization of activated carbon–metal oxide hybrid catalysts: new insights into reactions paths. J Mater Sci Technol. 2015;31:806–14.
29. Barroso-Bogeat A, Alexandre-Franco M, Fernández-González C, Macías-García A, Gómez-Serrano V. Electrical conductivity of activated carbon–metal oxide nanocomposites under compression: a comparison study. Phys Chem Chem Phys. 2014;16:25161–75.
30. Barroso-Bogeat A, Alexandre-Franco M, Fernández-González C, Gómez-Serrano V. Preparation of activated carbon-metal oxide hybrid catalysts: textural characterization. Fuel Process Technol. 2014;126:95–103.
31. Rouquerol F, Rouquerol J, Sing K. Adsorption by powders & porous solids. Principles, methodology and applications. London: Academic Press; 1999.
32. Silvestre-Albero J, de Salazar CG, Sepúlveda-Escribano A, Rodríguez-Reinoso F. Characterization of microporous solids by immersion calorimetry. Colloids Surf A. 2001;187–188:151–65.
33. Stoeckli F, Centeno TA. On the characterization of microporous carbons by immersion calorimetry alone. Carbon. 1997;35:1097–100.
34. Stoeckli F, Centeno TA. On the determination of surface areas in activated carbons. Carbon. 2005;43:1184–90.
35. Stoeckli F, Ballerini L. Evaluation of microporosity during activation of carbon. Fuel. 1991;70:557–9.
36. Rodríguez-Reinoso F, Martín-Martínez JM, Molina-Sabio M, Torregrosa R, Garrido-Segovia J. Evaluation of the microporosity in activated carbons by n-none preadsorption. J Colloid Interface Sci. 1985;106:315–23.
37. de Salazar CG, Sepúlveda-Escribano A, Rodríguez-Reinoso F. The use of immersion calorimetry to evaluate the separation ability of carbon molecular sieves. Stud Surf Sci Catal. 2000;128:303–11.
38. Barton SS, Evans MJB, Halliop E, MacDonald JAF. Acidic and basic sites on the surface of porous carbon. Carbon. 1997;35:1361–6.
39. Rodríguez-Reinoso F, Molina-Sabio M, González MT. Effect of oxygen surface groups on the immersion enthalpy of activated carbons in liquids of different polarity. Langmuir. 1997;13:2354–8.
40. Lopez-Ramon MV, Stoeckli F, Moreno-Castilla C, Carrasco-Marin F. On the characterization of acidic and basic surface sites on carbon by various techniques. Carbon. 1999;37:1215–21.
41. Rodríguez-Estupiñán P, Gómez F, Giraldo L, Moreno-Piraján JC. Immersion enthalphies in different liquids of activated carbons modified by surface chemistry. Mater Express. 2015;5:233–40.
42. Rodríguez GA, Giraldo L, Moreno JC. Calorimetric study of the immersion enthalpies of activated carbon cloths in different solvents and aqueous solutions. J Therm Anal Calorim. 2009;96:547–52.
43. Gómez F, Giraldo L, Moreno-Piraján JC. Granular activated carbons characterization by CO_2 adsorption isotherms and immersion enthalpy. J Therm Anal Calorim. 2015;120:1657–64.
44. Giraldo L, Moreno-Piraján JC. Relation between immersion enthalpies of activated carbons in different liquids, textural properties, and phenol adsorption. J Therm Anal Calorim. 2014;117:1517–23.
45. Acevedo S, Giraldo L, Moreno-Piraján JC. Enthalpies of immersion in benzene, cyclohexene and water of granular activated carbons prepared by chemical activation with solutions of $MgCl_2$ and $CaCl_2$. J Them Anal Calorim. 2015;121:1279–85.
46. Vargas DP, Giraldo L, Moreno-Piraján JC. Accessible area and hydrophobicity of activated carbons obtained from the enthalpy characterization. Adsorption. 2016;. doi:10.1007/S10450-015-97721-5.
47. Moreno-Piraján JC, Tirano J, Salamanca B, Giraldo L. Activated carbon modified with copper for adsorption of propanethiol. Int J Mol Sci. 2010;11:927–42.
48. Brunauer S, Emmet PH, Teller E. Adsorption of gases in multimolecular layers. J Am Chem Soc. 1938;60:309–19.
49. Dubinin MM. Physical adsorption of gases and vapors in micropores. In: Danielli JF, Rosenberg MD, Cadenhead DA, editors. Progress in surface and membrane science, vol. 9. New York: Academic Press; 1975. p. 1–70.
50. Setoyama N, Ruike M, Kasu T, Suzuki T, Kaneko K. Surface characterization of microporous solids with He adsorption and small angle X-ray scattering. Langmuir. 1993;9:2612–7.
51. Setoyama N, Suzuki T, Kaneko K. Simulation study on the relationship between a high resolution α_s-plot and the pore size distribution for activated carbon. Carbon. 1998;36:1459–67.
52. Rouquérol F, Luciani L, Llewellyn Ph, Denoyel R, Rouquérol J. Textures des matériaux pulvérulents ou poreux. Paris: Editions Techniques de l'Ingénieur; 2004.
53. Centeno TA, Stoeckli F. The assessment of surface areas in porous carbons by two model-independent techniques, the DR equation and DFT. Carbon. 2010;48:2478–86.
54. Bansal RC, Donnet JB, Stoeckli F. Active carbon. New York: Marcel Dekker; 1988.
55. Denoyel R, Rouquérol F, Rouquérol J. Porous texture and surface characterization from solid–liquid interactions: immersion calorimetry and adsorption from solution. In: Bottani EJ, Tascón JMD, editors. Adsorption by carbons. Amsterdam: Elsevier; 2008. p. 273–300.
56. Stoeckli F, Lavanchy A. The adsorption of water by active carbons, in relation to their chemical and structural properties. Carbon. 2000;38:475–7.
57. Centeno TA, Fernández JA, Stoeckli F. Correlation between heats of immersion and limiting capacitances in porous carbons. Carbon. 2008;46:1025–30.
58. Lide DR, editor. CRC handbook of chemistry and physics, 2005–2006. 86th ed. Boca Raton: Taylor & Francis; 2005.
59. Zhang M, Wu J, Lu DD, Yang J. Enhanced visible light photocatalytic activity of TiO_2 nanotube array films by co-doping with tungsten and nitrogen. Int J Photoenergy. 2013;. doi:10.1155/2013/471674.
60. Blanco J, Avila P, Yates M, Bahamonde A. The use of sepiolite in the preparation of titania monoliths for the manufacture of industrial catalysts. In: Martens J, Delmon B, Jacobs PA, Grange P, editors. Preparation of catalysts VI. Scientific bases for the preparation of heterogeneous catalysts. Amsterdam: Elsevier; 1995. p. 755–64.
61. Baes CF Jr, Mesmer RE. The hydrolysis of cations. New York: Wiley; 1976.
62. Salas-Peregrín MA, Carrasco-Marín F, López-Garzón FJ, Moreno-Castilla C. Adsorption of CO_2 on activated carbon from diluted ambient environments. Energy Fuels. 1994;8:239–43.